ACS APPLIED MATERIALS & INTERFACES

www.acsami.org

Research Article

Photodynamic Methylene Blue-Embedded Intragastric Satiety-Inducing Device to Treat Obesity

Sanghee Lee,[⊥] Ji Won Kim,[⊥] Jinhwan Park,[⊥] Hee Kyong Na, Do Hoon Kim, Jin Hee Noh, Dae Sung Ryu, Jae Myung Park, Jung-Hoon Park,* Hwoon-Yong Jung,* and Kun Na*

Cite This: https://doi.org/10.1021/acsami.2c00532

Read Online

ACCESS | Metrics & More | Article Recommendations | Supporting Information

ABSTRACT: Bariatric surgery is the most effective treatment for weight recidivism, and endoscopic bariatric treatment has been developed for a similar effect without anatomical modification. An intragastric satiety-inducing device (ISD) is a minimally invasive approach to induce satiety by continuously pressing the stomach and stimulating ghrelin-producing cells. To enhance the therapeutic effects of ISD, photodynamic therapy (PDT) can be combined by generating singlet oxygen under laser irradiation. Methylene blue (MB), as a photosensitizer (PS), was coated on the ISD surface for singlet oxygen production to stimulate or destroy cells. Ghrelin-producing cells effectively inhibited ghrelin secretion and induced gastrointestinal satiety signals compared with the MB-uncoated device via PDT. Herein, MB-embedded ISDs were developed, and their photoresponsive abilities were demonstrated in the device itself and in vitro. PDT with an MB-embedded ISD was successfully performed in a porcine model, which had 2-fold reduced body weight gain (12% in PDT vs 24% in control) and 2-fold reduced ghrelin levels (21.2 pg/mL in PDT vs 45.1 pg/mL in control) at the first week postprocedure. The simple and unique operation extends the point of view in PDT and is expected to be a novel endoscopic bariatric therapy.

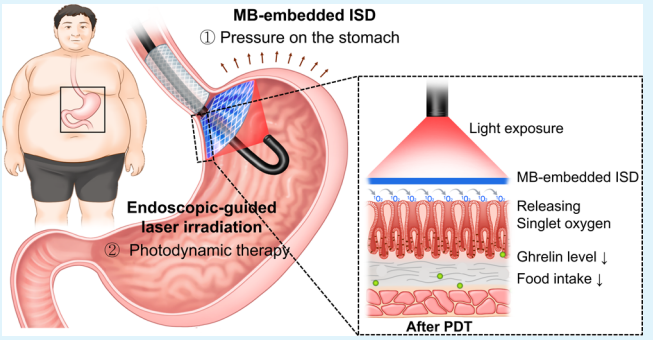

KEYWORDS: *methylene blue, photodynamic therapy, photodynamic stent, obesity, ghrelin*

1. INTRODUCTION

Obesity is a major public health concern globally and is linked to various metabolic and psychological problems, such as heart disease, stroke, diabetes, hypertension, and sleep disorders.[1−3] Endoscopic bariatric therapies, including intragastric balloons, endoscopic suturing devices, full sense devices, and bypass liners, have been developed as alternatives to bariatric surgery for high-risk obese patients and those who refuse surgery.[3−8] Recently, a new version named the intragastric satiety-inducing device (ISD) was developed and evaluated in rat and porcine models.[9−11] The ISD reduced food intake and suppressed weight gain with reduced ghrelin hormone levels.[10] However, device-related esophagogastric reflux, a high risk of migration into the stomach, and device-induced reversible inflammatory reaction with tissue hyperplasia were reported.[9,10] Although antimigration designs (i.e., barbs, flaps, and antireflux valves) were applied, these device-related complications were still inevitable.[10]

Ghrelin is known as a hunger hormone and a multifaceted gut hormone, especially the stomach, which activates the growth hormone secretagogue receptor.[12,13] Ghrelin signaling plays a significant role in increasing food intake,[12−14] and ghrelin-producing cells have been shown to have higher density and expression in the mucosa of obese patients.[15] The bariatric devices applying continuous pressure on the gastric cardia provided a feeling of satiety without food intake by suppressing ghrelin hormone resulting from stimulation of the ghrelin-producing cells, which are predominantly distributed in the gastric cardia.[16,17]

Photodynamic therapy (PDT) is a minimally invasive approach that induces cell death using reactive oxygen species (ROS).[18] Having extraordinary reactivity and a lifetime of 3.5 μs (at most 14 μs) in aqueous solution, ROS can rapidly attack surrounding cells and disappear without trace amounts.[19] Intracellular ROS levels induced by accumulated PS cause oxidative stress and lead to cell destruction.[20−22] These ROS properties suggest that PDT is a suitable minimally invasive treatment, and that PS enables the induction of cell death while being covered on the surface of the medical device.

Herein, we describe a PS-embedded ISD device for effectively reducing food intake and weight gain by suppressing

Received: January 10, 2022
Accepted: March 2, 2022

ghrelin hormone signaling by PDT. To collaborate ISD and PDT (Scheme 1), we coated nondegradable polymer

Scheme 1. Illustration of Photodynamic Therapy Using a Methylene Blue-Embedded Intragastric Satiety Inducing Device (MB-Embedded ISD)[A]

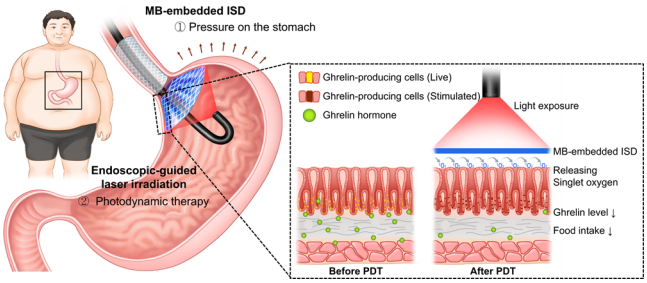

[A]MB-embedded ISD transplanted in the cardia portion of the stomach was located in ghrelin-producing cells. ISD mechanically pressured the gastric nerve, which signals a feeling of fullness to the brain. Under light exposure, MB-contacted ghrelin-producing cells generated singlet oxygen to stimulate or destroy cells, inducing a decrease in plasma ghrelin levels and loss of appetite. This series of procedures can be a novel minimally invasive treatment for obese patients to lose weight.

(silicone) and PS (methylene blue, MB) on the disk portion of the ISD. MB, a generally FDA-approved drug, is applied in the treatment of methemoglobinemia.[23,24] Endoscopically applied MB selectively stains intestinal metaplasia and dysplasia in dark blue. MB has been studied in various clinical cases, including the treatments of melanoma, basal cell carcinoma, virus, and fungal infections, due to its low toxicity and side effects.[25−27] Furthermore, the photoresponsiveness of MB to white light slightly stimulates the formation of singlet oxygen species.[28] To increase their photoactivity, red light (approximately 660 nm) with a maximum absorbance of MB at their wavelength may be used. MB-embedded ISD was successfully placed on target tissue and irradiated with a specific wavelength laser, generating singlet oxygen to induce cell death or stimulation of connected cells. Furthermore, it is expected that various ISD-related complications can be significantly decreased by reducing the indwell time of ISD.

In this study, MB-embedded ISD was developed by the optimized materials and blending ratio. The photoresponsibility of MB remained after embedding in silicone, and ROS caused obvious cytotoxicity in cells connected with MB-embedded ISD. Furthermore, the possibility of repeat treatment was validated based on the low MB loss and the maintained singlet oxygen generating efficacy. Finally, in an in vivo porcine model, minimally invasive PDT using MB-embedded ISD, including weight changes, changes in ghrelin levels, and histological changes over time after PDT, demonstrated the effectiveness and safety of a newly developed PDT therapeutic strategy for obesity. This research proposes an innovative bariatric device that can alternate and supplement bariatric surgery for morbidly obese individuals, stimulating ghrelin-secreting cells with ROS generated from MB.

2. MATERIALS AND METHODS

2.1. Materials. Methylene Blue (MB, Cat. 66720), methanol (MeOH), xylene, 3-(4,5-dimethyl-2-thiazolyl)-2,5-diphenyl-2H-tetrazolium bromide (MTT), and trypan blue were purchased from Sigma−Aldrich Co. (St. Louis, MO). Silicone derivatives (MED-6640) were purchased from Nusil Technology LLC. (Carpinteria, CAMA, USA). The ISD and its delivery system were supplied by S&G Biotech (Yongin, Gyeonggi-do, Korea).

2.2. Fabrication of MB-Embedded ISD. MB was dissolved in chloroform, isopropyl alcohol, ethanol, acetonitrile, acetone, MeOH, dimethyl sulfoxide, and dimethylformamide (2 mg/mL). The solubility of MB in various solvents was confirmed by the Tyndall phenomenon. To optimize the ratio of xylene and MeOH, MB was dissolved in mixed solvents depending on the volume ratio (0.1 mg/mL in 1 mL). MB−silicone solution is composed of silicone (768 mL), xylene (192 mL), and MeOH with MB (40 mL, at 0.5 mg/mL). MB−silicone solution with unimproved solubility was blended only with xylene without MeOH.

The ISDs used in this study are described in detail in previous studies.[9,10] In brief, the ISD consisted of an uncovered straight self-expandable metallic stent for the lower esophagus and a silicone-covered nitinol disk for the cardia portion of the stomach. When fully expanded, the esophageal part was 24 mm in diameter and 60 mm in length. The disk part was a double star-shaped flat mesh 75 mm in diameter. The disk was connected to the distal end of the esophageal part by two 50 mm long nitinol wires. For the fabrication of MB-embedded ISD, the dip coating technique was used. The disk part of ISD was dipped in the MB−silicone solution for 20 s and slowly withdrawn. It was immediately dried in an oven at 150 °C for 2 h and air-dried for 30 min at room temperature.

To make the ISD removable, a nylon braided string (diameter: 2 mm, Mepfill-UPE, Metabiomed, Co. Ltd., Osong, Korea) was hooked inside two bends of the proximal end of the esophageal part. The MB-embedded ISD was loaded at a 28 Fr black Teflon sheath to prevent light exposure. The delivery system comprised the black Teflon sheath and a pusher catheter with a guiding olive tip. The total length of the delivery system was 120 cm. MB-embedded ISD was made by our specifications (S&G Biotech, Yongin, Korea) and is not commercially available elsewhere.

2.3. ROS Generation of MB and MB-Embedded Stent Piece. The ROS generation efficacy was measured by singlet oxygen sensero green (SOSG). SOSG was diluted in distilled water at 10 μM, and MB was dissolved in this solution at a concentration of 5 μg/mL (2 mL). To confirm the photodynamic response of MB, a 670 nm laser source (Fiber Coupled Laser Modules, LaserLab, Seoul, Korea) was irradiated with 20 mW/cm^2 for 20 s. The fluorescence intensity of SOSG (λ_{ex} = 504 nm, λ_{em} = 525 nm) was detected using fluorescence spectroscopy (RF-5301, Shimadzu, Kyoto, Japan).

MB-embedded ISD pieces were made to demonstrate the ROS generation effects of MB coated on the stent surface. The stent strut was fragmented into 4-cell pieces (1 cm × 1 cm, 1 cm^2) and dip-coated in MB−silicone solution (MB conc. 0.05, 0.10, 0.50, and 1.00 mg/mL). These pieces were dropped down the SOSG solution and irradiated with a laser (20 mW/cm^2, 20 s, 10 J/cm^2). The experiments immediately after coating were designated as the first test (first), and then the second test (second) was performed after rinsing in buffer for 24 h and the third (third) after rinsing for another 24 h (accumulative 48 h). The ROS generation efficacy of MB-embedded ISD was simulated following this procedure.

2.4. Cell Culture and Incubation Conditions. Mouse connective tissue cells (L929, KCLB no. 10001) and human stomach cells (AGS, KCLB no. 21739) were obtained from the Korean Cell Line Bank (KCLB). L929 and AGS cells were cultured in RPMI 1640 medium containing 10% heat inactivated fetal bovine serum and 1% antibiotics (penicillin/streptomycin). All of the cell culture supplements were purchased from HyClone (Logan, UT). Cells were cultured at 37 °C in a humidified atmosphere with 5% CO_2 and subcultured in fresh medium every 2 to 3 days.

2.5. In Vitro Cytotoxicity and Phototoxicity of MB-Embedded ISD. L929 and AGS cells were seeded in a 48-well cell culture plate at a density of 2 × 10^4 cells/well (200 μL per well) and allowed to attach for 24 h. Cells were incubated with MB diluted in serum-free medium (conc. 0.25, 0.50, 1.00, 2.50, 5.00, 10.00, 25.00, and 50.00 μg/mL) for 4 h. After adequate washing with Dulbecco's

https://doi.org/10.1021/acsami.2c00532
ACS Appl. Mater. Interfaces XXXX, XXX, XXX−XXX

phosphate-buffered saline (DPBS), fresh culture medium was added. In cytotoxicity, cells were not laser irradiated. In contrast, in phototoxicity, cells were irradiated with a 670 nm laser (50 mW/cm^2, 100 or 200 s, 5 or 10 J/cm^2). After incubating for 24 h, MTT solution (1 mg/mL) was added to each well and incubated for 4 h. Then, the medium was replaced with dimethyl sulfoxide to dissolve living cells. The absorbance of the MTT dye at 570 nm was measured using a microplate reader (Biotek Instruments Inc., Winooski, VT).

AGS cells were seeded in a 12-well cell culture plate at a density of 5×10^5 cells/well (500 μL per well). After incubating for 24 h, the medium was removed, and MB-embedded ISD pieces were placed on the cell monolayer in each well. Each piece was irradiated with light from the top of the cell culture plates (power; 50 mW/cm^2, time; 20, 60, or 100 s, total energy; 1, 3, or 5 J/cm^2). After irradiation, 1 mL of fresh medium was added, pieces were removed, and the cells were incubated for 30 min. The dead cells were stained with 0.4% trypan blue solution for visualization. The stained cells and their morphology were observed under an optical microscope (ICX40, Ningbo Sunny Instruments Co., Ltd., Zhejiang, China) at 40× magnification.

2.6. Evaluation of Maintained MB. MB-embedded ISD was immersed in cosolvent (xylene:MeOH = 7:3, volume ratio) and stirred at 250 rpm for 48 h in an orbital shaker to fully elute coated MB. The total eluted amount of MB was quantified at 667 nm by UV−vis spectroscopy (UV-2450, Shimadzu, Kyoto, Japan). The area of the stent was measured and then represented as mass per unit area (μg/cm^2). MB-embedded ISD was sunk in 0.01 M phosphate buffer saline (pH 7.0, 5 mL) and stirred at 50 rpm for 2 weeks (at 37 °C). Buffer saline was regularly withdrawn and replaced with fresh solution. The released amount of MB was analyzed by UV−vis spectroscopy at 667 nm. The residual percentage of MB on the surface was calculated by the following equation.

$$\text{residual percent}(\%) = 100 - \left(\frac{\text{released amount of MB}}{\text{total eluted amount of MB}} \times 100 \right)$$

The surface of MB-embedded ISD was observed by field emission scanning electron microscopy (FE-SEM) (Hitachi S-4800, Tokyo, Japan). The surface was confirmed before and after release for 2 weeks. For observation with FE-SEM, stents were sliced, mounted, sputter-coated by an ion coater, and analyzed at an accelerating voltage of 3 kV.

2.7. Animal Study. This study was approved by the Institutional Animal Care and Use Committee of our institution and conformed to U.S. National Institutes of Health guidelines for humane handling of laboratory animals. A total of five juvenile pigs weighing 32−35 kg (median, 34.56 kg) (International Animal Experiment Center, Pocheon, Korea) were used. Four pigs underwent PDT using MB-embedded ISD. The remaining weight- and age-matched healthy pig was used as a control. All pigs were fed a fixed amount of food (regular chow; 3 kg per day) and were maintained at 22 ± 2 °C. The four pigs were sacrificed immediately and 1, 2, and 4 weeks after PDT. The control pig was sacrificed at 4 weeks. All pigs were euthanized with 75 mg/kg potassium chloride via marginal ear vein injection after follow-up studies.

2.8. Photodynamic Therapy Using MB-Embedded ISD. The techniques of ISD placement and removal have been described in detail previously.[10] After 24 h of fasting, pigs were anesthetized using a mixture of 50 mg/kg zolazepam and 50 mg/kg tiletamine (Zoletil 50; Virbac, Carros, France) and 10 mg/kg xylazine (Rompun; Bayer HealthCare, Leverkusen, Germany). An endotracheal tube was placed, and anesthesia was administered by inhalation (0.5−2% isoflurane (Ifran; Hana Pharm. Co., Seoul, Korea) with oxygen (510 mL/kg per min) at 1:1). An endoscope (CF-H260AI; Olympus Inc. Tokyo, Japan) with an overtube (Guardus Overtube; STERIS, Mentor OH) was advanced through the mouth to the stomach, suction of gastric secretions was performed, and the endoscope was removed with the overtube left in place. A 0.035-in. guidewire (Radifocus M; Terumo, Tokyo, Japan) was inserted through the overtube into the stomach. The MB-embedded ISD delivery system was passed over the guidewire into the stomach under fluoroscopic guidance. The pusher catheter was held in place, while the sheath was slowly withdrawn in continuous motion. The disk part was placed in the gastric fundus, and the connection part was placed in the lower esophagus, bridging the gastroesophageal junction. Endoscopic examination was performed to confirm whether the disk part and the gastric cardia were tightly attached. An optic fiber (Fiber optic cable, Biolitec MILON Group, UK) was inserted through the working channel of the endoscope. Laser irradiation with a wavelength of 633 nm was carried out at a power density of 1000 mW/cm^2 and an irradiation energy dose of 200 J/cm^2 using a diode laser system (DIOMED 630, Biolitec MILON Group, UK). MB-embedded ISD was immediately removed after PDT through the overtube. Antibiotics (cefazolin, 15 mg/kg) and analgesia (alfentanil, 0.5 mg) were administered for 3 days after the procedures.

2.9. Histological Analysis. Surgical exploration of the lower esophagus and the entire stomach was performed. The mucosal injuries, bleeding, and ulceration caused by PDT were evaluated by gross examination. The excised tissue samples were then fixed in 10% buffered formalin for 24 h and embedded in paraffin. The paraffin blocks were sectioned. The slides were stained with hematoxylin and eosin (H&E) and Masson's trichrome (MT) to evaluate inflammatory cell infiltration and the degree of fibrotic changes.

Immunohistochemistry (IHC) was performed on paraffin-embedded sections with terminal deoxynucleotidyl transferase-mediated dUTP nick and labeling (TUNEL; ApopTag, Qbiogene, Darmstadt, Germany) and antighrelin (ab104307, Abcam, Cambridge, UK) as the primary antibodies. The sections were visualized with a BenchMark XT IHC automated immunohistochemical stainer (Ventana Medical Systems, Tucson, AZ).

2.10. Follow-Up and Total Body Weight Gain Analysis. All pigs were monitored daily for any behavioral changes and degree of diet. Endoscopic examination was performed before sacrifice to evaluate the mucosal injuries at the fundus of the stomach. Body weight was monitored weekly, and the percentage of total body weight gain (%TBWG) was calculated as follows:[9,10] total body weight gained each week/baseline weight ×100.

2.11. Ghrelin Analysis. Plasma levels of ghrelin hormone (Bertin Bioreagent, acetylated ghrelin (pig), EIA kit, Rockville, MD) were assessed weekly before consuming the morning meal after fasting overnight for 8 h. Blood samples were collected in tubes containing plasma separator tubes and a protease inhibitor to prevent the degradation of acetylated ghrelin. The collected blood samples were separated only by serum and stored immediately at −20 °C until the time of assay.

2.12. Statistical Analysis. Data are expressed as the mean ± standard deviation. Significance was determined using analysis of variance (ANOVA) and one-tailed Student's t test. Significance was noted as follows: **, $P < 0.01$; ***, $P < 0.001$.

3. RESULTS AND DISCUSSION

3.1. Optimization of MB-Embedded ISD. MB was well-dissolved in polar protic solvents (i.e., water, ethanol, MeOH, etc.), but not in organic solvents (i.e., xylene, tetrahydrofuran, dichloromethane, etc.). Silicon carbide-coated stents have low restenosis and thrombosis rates, which is possible if various types of silicone molecules are homogeneously dispersed in xylene.[29,30] These steps later affect the coating performance, the physical properties of the stent, and the loss of MB over time. However, MB cannot be dispersed in xylene at all (Figure 1A). To consistently blend MB and silicone, cosolvents were selected in consideration of the following conditions: (i) miscible with xylene, (ii) extremely volatile, and (iii) MB-soluble solvents. Other candidates include chloroform, acetone, ethanol, acetonitrile, isopropyl alcohol, dimethyl sulfoxide, dimethylformamide, and MeOH (Supporting Information (SI) Figure S1). Solvent dissolved MB without any agglomerates was selected at 20% (v/v) solution in xylene, and it was MeOH. To minimize the amount of MeOH, it was

https://doi.org/10.1021/acsami.2c00532
ACS Appl. Mater. Interfaces XXXX, XXX, XXX−XXX

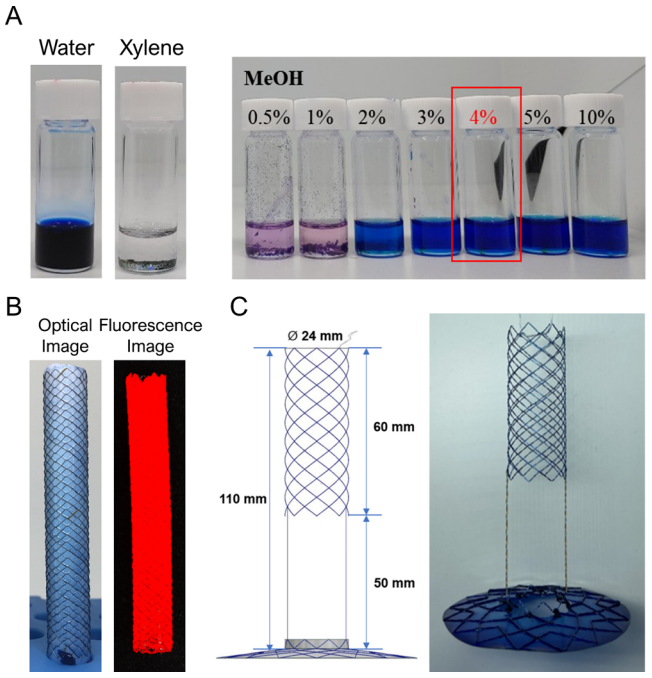

Figure 1. Fabrication of MB-embedded ISD. (A) A photograph of MB solution in water and xylene (left). Solubility of MB in xylene was improved by adding MeOH (MB concentration; 2 mg/mL, vol %) (right). (B) Optical and fluorescence images of stents coated with MB (MB concentration in coating solution; 0.50 mg/mL). (C) Schematic reference and actual appearance of MB-embedded ISD. MB was coated only on the disk part.

confirmed whether aggregates were formed by decreasing the MeOH portion, resulting in the occurrence of precipitates from less than 4%. In the optimized recipe, MB was dissolved in MeOH, and both xylene and silicone were added to reach final concentrations of 0.05, 0.10, 0.50, and 1.00 mg/mL, with a mixture volume ratio of 1:1:0.5 (silicone A:silicone B:xylene, vol %). The MB coating layer consisted of 76.8% silicone, 19.2% xylene, and 4% MeOH containing MB. The uniformity of MB coating on the stent surface was confirmed by optical and fluorescence images (Figure 1B). In Figure 1C, the actual MB-embedded ISD is shown based on a schematic image. Only the disk part was coated with MB, and the esophageal part was left uncoated. This is because the disk part connected with the fundus, where ghrelin-secreting cells are located, needs photoactivity, but unexpected events might occur if the esophageal part was also coated.

3.2. ROS Generation for Photodynamic Effects. MB absorbs red region light (suitable excitation wavelength, λ_{max} = 665 nm).[31] To confirm ROS generation efficacy in the uncoated state, MB (5 μg/mL) was irradiated with a laser while coincubating with SOSG (SI Figure S2). As the laser intensity increased, the fluorescence intensity of SOSG was increased under aqueous conditions. Based on ROS formation, we assessed the phototoxicity of MB at various doses in L929 (normal cells) and AGS (stomach cells) cells using the MTT assay (Figure 2A). In both cell lines, MB-treated cells showed approximately 75% cell viability without laser irradiation. The cells overly take up MB because MB has a strong positive charge such that it can strongly interact with the anionic charged cellular membrane in vitro. In the presence of light,

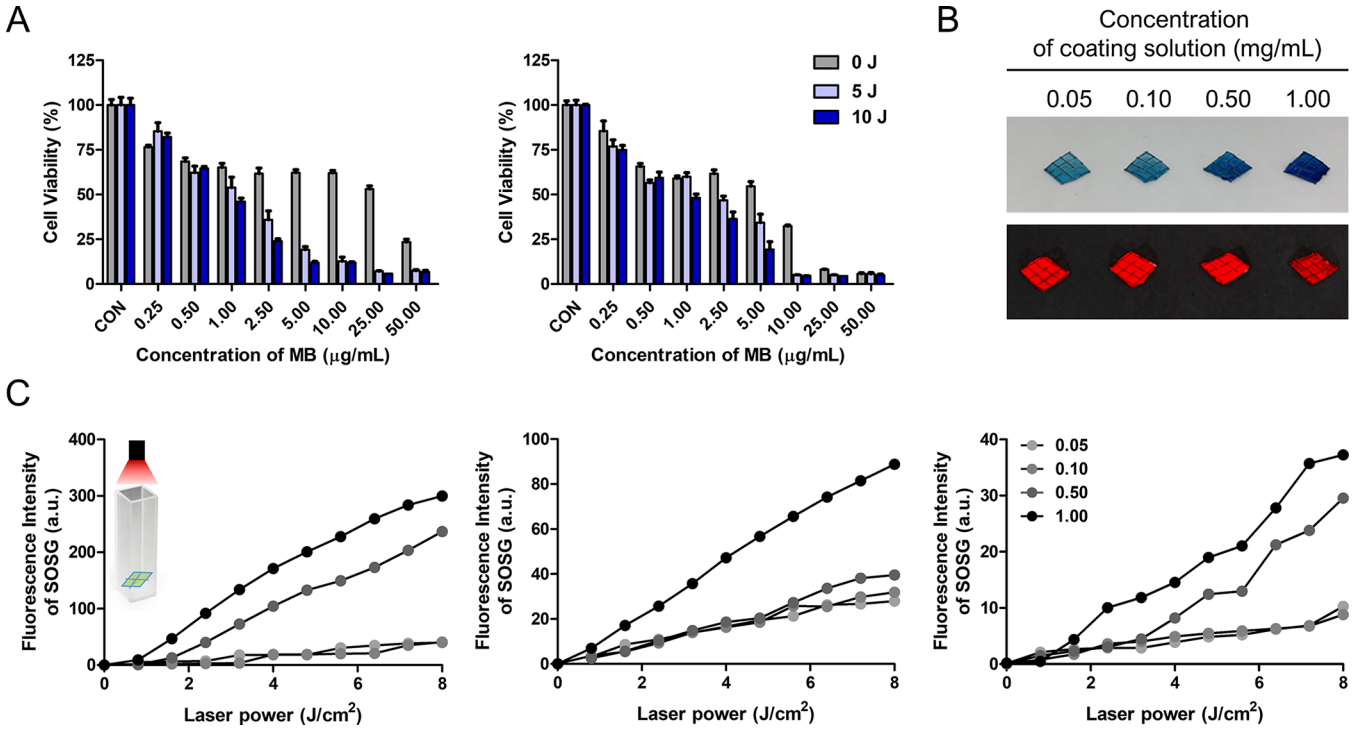

Figure 2. ROS generation for photoactivity. (A) Phototoxicity of MB determined by MTT assay at various concentrations under laser irradiation at 0, 5, and 10 J/cm^2 in L929 (normal cells) and AGS (stomach cells) (n = 4). (B) Optical and fluorescence images of stent pieces coated with MB (MB concentration of coating solution; 0.05, 0.10, 0.50, 1.00 mg/mL). (C) Repeated ROS generation efficacy of MB-coated stent pieces in water (n = 3). SOSG assay was carried out immediately after making the pieces (1st), and the same pieces were eluted in PBS for 24 h (followed by a second measurement, 2nd). The 3rd measurement was performed after eluting for an additional 24 h in the same manner. The concentration corresponded to the MB of the coating solution.

https://doi.org/10.1021/acsami.2c00532
ACS Appl. Mater. Interfaces XXXX, XXX, XXX−XXX

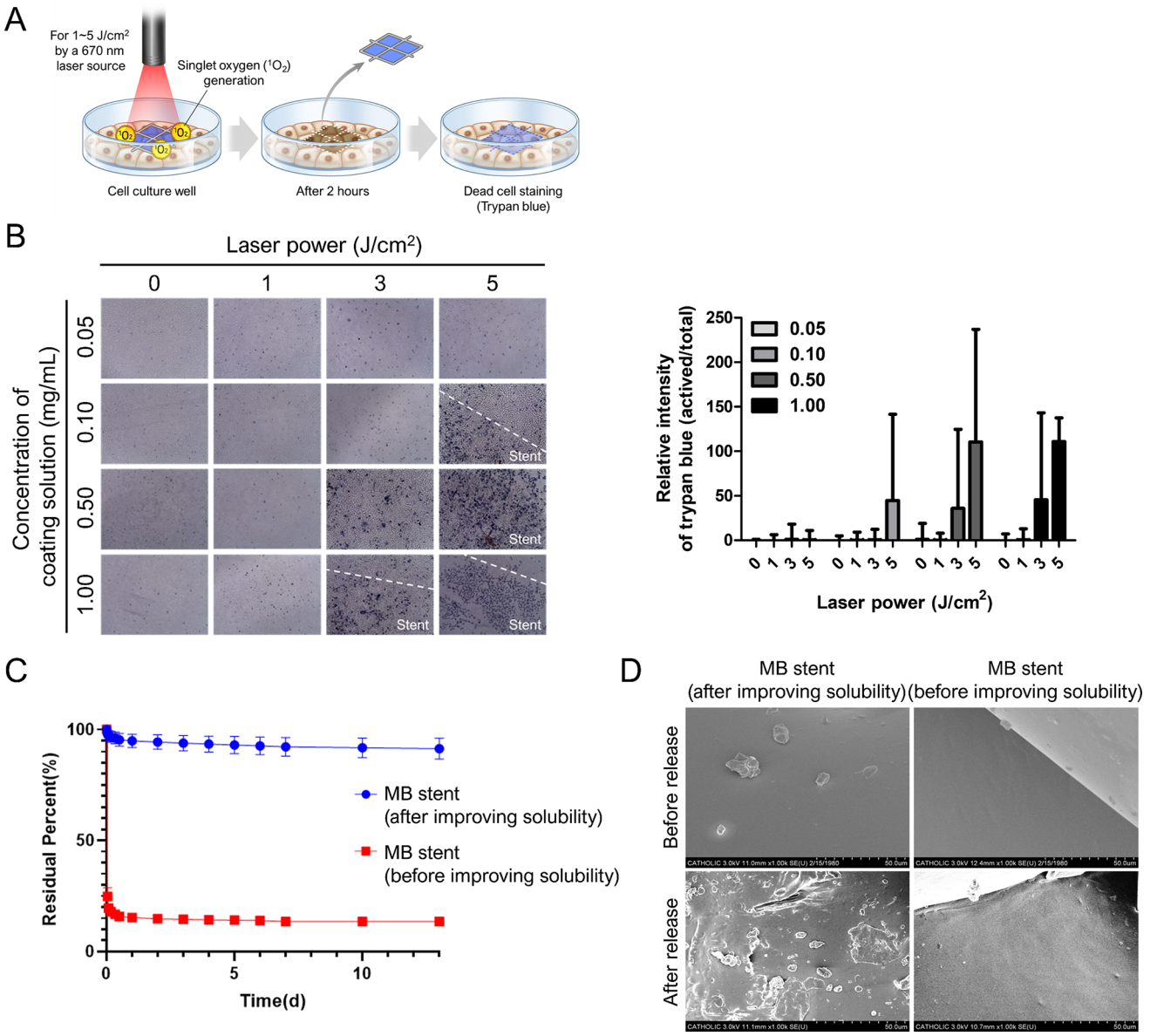

Figure 3. Photodynamic effects of MB-coated stent pieces and residual MB on the surface. (A) Schematic illustration of in vitro test. MB-coated pieces were placed on the cell monolayer, and the laser was irradiated. (B) Trypan blue staining to confirm dead cells via ROS (left). The bar graph indicates trypan- blue-stained cells through analysis via ImageJ software (based on activated pixels/total pixels) (right). (C) Comparison of MB loss rate from the stent surface according to solubility improvement by MeOH (incubated in PBS, 37 °C, 50 rpm). (D) SEM images to compare the change of the surface before and after release according to the solubility improvement by MeOH (scale bar; 50 μm).

higher light energy results in lower cell viability. At 5 μg/mL MB, L929 cell death increased by 1.8 times at 5 J and 2.0 times at 10 J. Stent pieces were fabricated to confirm that the photoresponsivity of coated MB was maintained despite being embedded in silicone. Additionally, repeatability is an important feature of PDT because further PDT has no accumulative destructive effect and does not genitively influence laser radiation.[32] Both MB-embedded silicone and the repeatability of PDT were demonstrated depending on the concentration (coating solution concentration of MB; 0.05, 0.10, 0.50, and 1.00 μg/mL, as shown Figure 2B) by the SOSG test with laser irradiation (Figure 2C). Since MB will be naturally eliminated from the body, the second test was conducted after incubation in mimetic body conditions for 24 h, and the third test was performed after an additional 24 h. It was demonstrated that the higher MB concentration of the coating solution generated a greater amount of ROS. The SOSG increase was observed even after the third repetition, demonstrating that repeated treatment is possible during the device implant period simply by light irradiation. Repeated PDT is possible without additional PS administration by simply irradiating light while the stent is transplanted so that it is possible to maximize therapeutic effects and personalize treatment.

3.3. In Vitro Photodynamic Effects of MB-Embedded ISD. In conventional PDT, PS accumulates inside the cell and induces apoptosis via ROS generation under light. However, in PDT-medical devices, PS is located outside the cellular membrane. Although the mobility distance of ROS is approximately 400 nm, which is shorter than the size of a single cell, it is a distance that can penetrate the cell membrane and damage the cell.[33−35] In other words, PS does not

https://doi.org/10.1021/acsami.2c00532
ACS Appl. Mater. Interfaces XXXX, XXX, XXX−XXX

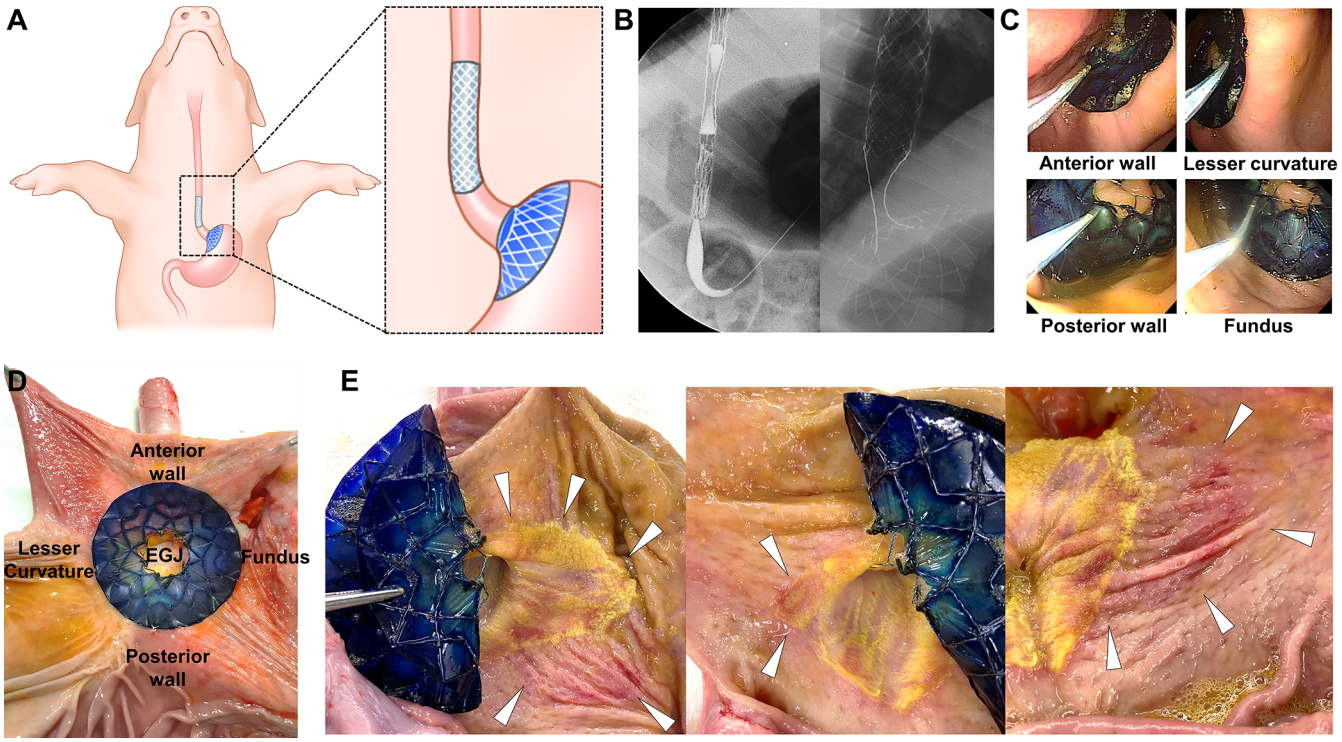

Figure 4. PDT with use of MB-embedded ISD in a porcine model. (A) Schematic illustration of the placed MB-embedded ISD into the stomach of pigs. (B) Radiographic images showing the technical steps of MB-embedded ISD in a porcine model. (C) Endoscopic images obtained during laser irradiation showing the four sections based on the anatomical structure. (D) Photograph obtained from pigs immediately sacrificed after PDT showing the placed MB-embedded ISD and mucosa of the gastric cardia portion of the stomach. (E) Photographs showing mucosal injuries and ulceration (arrowheads) at the cardia portion of the stomach in sacrificed pigs immediately after the PDT procedure.

necessarily exist in intracellular systems but can sufficiently disturb the cell only when in contact with the cellular membrane.[36,37] In our previous studies,[36] we demonstrated that PS successfully produced ROS in the extracellular system, which exerted PDT effects. As shown in Figure 3A, to prove the in vitro photoresponsive effects of the MB-embedded ISD, MB-coated pieces were placed on the AGS cell monolayer and subsequently irradiated with a laser above the pieces. Dead cells could be visualized by staining with trypan blue, which penetrates the dead cell membrane but not living cells (Figure 3B). Trypan-blue-stained cells were analyzed via ImageJ software. Stent pieces coated with 0.10 mg/mL MB−silicone solution showed phototoxicity after 5 J/cm^2 laser treatment. Additionally, those coated with 0.50 or 1.00 mg/mL caused cell death when irradiated with more than 3 J/cm^2. Overall, blue-stained cells were significantly detected as the laser intensity increased. An important point is that dead cells were observed only surrounding the stent area, but the cells were alive in the uncontacted area. This result implies that, in the in vivo models, we can selectively kill only directly contacted cells with the surface of the stent through accurate laser irradiation after strutting the MB-embedded ISD.

3.4. Evaluation of MB Retained on Surface. MB has a risk of escaping from the device surface due to its water-soluble properties. Therefore, it is important to homogeneously coat MB to improve its solubility, preventing MB washout and unexpected cytotoxicity. This issue was relieved by fixing MB into silicone molecules. The advantages of combining MB and silicone were demonstrated through the evaluation of residual MB on the surface using both stents coated with MB in the aggregated state (so-called before improving solubility) and stents coated with urethane (MB−urethane, the other nondegradable polymer). MB-embedded ISD contained 39.4 μg/cm^2 MB before improving solubility, but after improving solubility, MB covered 255.4 μg/cm^2. The unimproved MB stents were not fully coated in the dip coating process due to aggregates and precipitates of MB. After 13 days of incubation in PBS (50 rpm, 37 °C), the residual percentages of MB were 91.41% (improved solubility) and 13.6% (unimproved solubility) (Figure 3C, detailed in SI Table S1). The stent surface was observed using SEM images to analyze the smoothness before release and changes during spontaneous release (Figure 3D). As shown by the unimproved MB−stent surface, MB was largely aggregated before release, and the surface appeared rougher after release. On the other hand, in the case of the improved MB stent, MB agglomerates were hardly discovered, but the smooth surface was maintained even after release. In addition, the MB−urethane stent captured 538.0 μg/cm^2 MB and remained at 14.4% after release (SI Figure S3). Urethane instantly captured a large amount of MB due to its high volatility at room temperature compared with silicone carbide. Taken together, silicone was a suitable nondegradable polymer to coat the stent, and the optimization of silicone and MB coating solvent was essential for the long-term retention of MB in the body.

3.5. Technical Outcomes of Animal Study. MB-embedded ISD was successfully placed in all pigs without any procedure-related complications (schematic images in Figure 4A, fluoroscopic images to show the located ISD in Figure 4B). Endoscopic examination immediately after MB-embedded ISD placement confirmed that the MB-embedded disk part and the gastric cardia were tightly attached. Finally,

https://doi.org/10.1021/acsami.2c00532
ACS Appl. Mater. Interfaces XXXX, XXX, XXX−XXX

PDT was successfully performed under endoscopic guidance in all pigs. The MB-embedded ISD was also successfully removed under fluoroscopic and endoscopic guidance immediately after PDT. All pigs survived until the end of the study without PDT-related complications. Based on the anatomical structure, the place disk part was irradiated for four consecutive sessions for a total of 800 s (200 s for each section) (SI Figure S4). Laser irradiation at a power density of 1000 mW/cm^2 and an irradiation energy dose of 200 J/cm^2 were performed on the four sections based on the anatomical structure over 200 s in each section (Figure 4C–E). A single power of PDT was used in this study, and additional research is needed to find optimal laser power in a rodent model to increase the sample size of animals. A commercially available laser system with cylindrical optic fiber was used for PDT in this study. Further investigation to develop an optimal design of an optic fiber for the gastric cardia was also required to increase the PDT effect with uniformly distributed laser irradiation.

3.6. Autopsy and Histological Findings. The excised specimens showed mucosal injuries and ulceration at the cardia portion of the stomach in sacrificed pigs immediately and 1 week after the PDT procedure (Figure 5). However, definite mucosal injuries were not observed in sacrificed pigs at 2 and 4 weeks. H&E-stained tissue sections at the esophagus and esophagogastric junction did not differ between the control and PDT-treated groups and did not show any abnormalities on microscopic examination (SI Figure S5). Severe submucosal lymphoid follicular hyperplasia, moderate epithelial hyperplasia with hyperkeratosis, and increased inflammatory cell infiltration were observed in the pigs immediately sacrificed after PDT. These findings gradually recovered from the first to the fourth week. At week 4, there was no difference from the control findings except epithelial hyperplasia. In MT-stained tissues, the degree of collagen deposition was increased in the PDT-treated pigs compared with the control pig. TUNEL-positive deposition also markedly increased in PDT-treated pigs, while it gradually recovered for 4 weeks. TUNEL-stained tissues of PDT-treated pigs indicated that controlled ROS release led to cell damage to extra normal tissues and induced apoptosis with inflammatory reactions. However, damaged cells gradually regenerated over time because PDT with MB-embedded ISD is postulated to cause relatively less damage, sparing the surrounding structures, such as blood vessels or nerves, which results in rapid regeneration of the PDT-treated tissues. Antighrelin positive deposition in control pigs was prominently higher than that in PDT-treated pigs, and this positive deposition gradually increased over time. Consistent with the changes in the plasma ghrelin level, antighrelin positive deposition decreased immediately after PDT compared with the control pig. Single PDT successfully stimulated ghrelin-producing cells, which were predominantly distributed in the gastric cardia, resulting from suppression of antighrelin positive deposition.

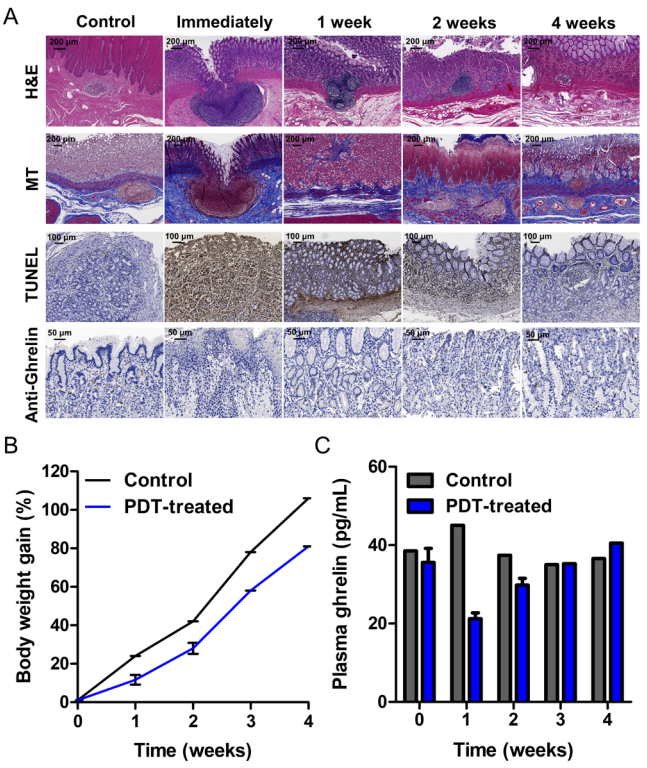

Figure 5. In vivo therapeutic effects for MB-embedded ISD. (A) Representative microscopic images obtained immediately and 1 week, 2 weeks, and 4 weeks after PDT with MB-embedded ISD of hematoxylin and eosin (H&E, magnification ×5), Masson's trichrome (MT, magnification ×5), TUNEL (magnification ×10), and anti-ghrelin (magnification ×20) staining at the gastric cardia portion in control and PDT-treated pigs. (B) The percentage of total body weight gain (%TBWG) in PDT-treated pigs was lower than that of the control pig at the first (12% vs 24%), second (28% vs 42%), third (58% vs 78%), and fourth weeks (81% vs 106%). (C) The plasma ghrelin level in three PDT-treated pigs was decreased compared with that in the control pig at the first and second weeks. There was no difference between the two groups at the third and fourth weeks.

3.7. Weight Changes. Weight gain was observed in all pigs. The PDT-treated pigs had a lower %TBWG than that of the control pig at the first (12% vs 24%), second (28% vs 42%), third (58% vs 78%), and fourth weeks (81% vs 106%) (Figure 5B). The %TBWG of the ISD group in the previous study was 4%, 15%, 29%, and 49% from the first to the fourth week.[10] Compared to the previous study with ISD placement, the weight loss effect was shown at 1 and 2 weeks after PDT, but weight gain showed a similar tendency to that of the control group. Weight changes and food intake in animal studies might be imprecise due to various environmental factors, such as behavior during food intake, stress, and postprocedural influence. Although a fixed amount of food was provided, the measurement of the actual food intake was very vague. Pigs tended to play with the food with their nose, so it was difficult to accurately measure the amount of the food being eaten. The results of weight changes in the present study indicated that repeated and periodic PDT, specifically at a 2-week interval, seems to be necessary to maintain the weight loss effect in a porcine model.

3.8. Plasma Ghrelin Level Changes. As shown in Figure 5C, there was no significant difference in the initial plasma ghrelin level between the two groups (control vs PDT: 38.5 pg/mL vs 35.6 ± 3.6 pg/mL). The ghrelin level in three PDT-treated pigs (21.2 ± 1.5 pg/mL) was relatively decreased compared with that in the control pig (45.1 pg/mL) in the first week. This difference was maintained at the second week (37.4 pg/mL in control pig vs 29.8 pg/mL in two PDT-treated pigs). There was no difference between the two groups at the third week (35 pg/mL in control pig vs 35.3 pg/mL in PDT-treated pig) and the fourth week (36.6 pg/mL in control pig vs 40.5 pg/mL in PDT-treated pig). Consistent with the weight change findings, plasma ghrelin changes demonstrated

https://doi.org/10.1021/acsami.2c00532
ACS Appl. Mater. Interfaces XXXX, XXX, XXX−XXX

significantly less at the first and second weeks after PDT; however, the level was similar to that of the control pig at the third and fourth weeks. PDT with MB-embedded ISD at the cardia portion of the stomach led to decreased ghrelin levels until 2 weeks by stimulation of ghrelin-producing cells. Ghrelin has been related to inducing appetite and feeding behaviors, and injections of ghrelin in both humans and rats have been shown to increase food intake.[14,17] Ghrelin-producing cells are predominantly located in the fundus of the stomach and directly stimulate appetite and induce positive energy balance, resulting in weight gain.[38,39] Bariatric embolization into the gastric arteries that supply the fundus can significantly suppress ghrelin levels with a 55% reduction from baseline levels and weight gain over an 8-week period.[40,41] The current bariatric devices have to be placed into the gastroduodenal for a certain period to treat obesity, and various devices-related complications frequently occurred such as migration and ulcer formation.[1,3,4,7,8] The advantage of our strategy was that devices-related complications can be significantly reduced by eliminating the indwell time of ISD. Body weight and ghrelin hormone after single PDT with MB-embedded ISD demonstrated significantly less at the first and second weeks without any procedure-related complications; however, the levels were gradually recovered. The efficacy of PDT can be maintained with repeated PDT procedures. Although the repeatable procedure can be a disadvantage in real clinical applications, this procedure was easy and safe therapeutic strategy under endoscopic guidance to decrease ghrelin level compared to previous studies.[9,10,40,41]

4. CONCLUSION

In summary, we demonstrated MB-embedded ISD to enhance the existing ISD effects and shorten the period of device implantation, thereby reducing concerns about migration. To homogeneously cover MB, a suitable combination of solvents and their ratio were attained, and the MB concentration at which ROS could have therapeutic effects was selected. From the perspective of PDT, MB-embedded ISD has greater significance, which means improvement of the bioavailability of PS and better practicality in laser irradiation. In addition, definite histological changes showed reduced ghrelin levels due to mucosal stimulation at the cardia. This effect was maintained for 2 weeks after the PDT procedure; however, the hormone level after 3 to 4 weeks was similar to that of the control pig, and histological changes also gradually recovered over time. These findings supported that repeated PDT with an interval of 2 weeks is required to maintain weight loss and hormone reduction for long-term efficacy. However, additional investigation is required to evaluate the efficacy and safety of repeated PDT using MB-embedded ISD for the treatment of obesity.

■ ASSOCIATED CONTENT

Supporting Information

The Supporting Information is available free of charge at https://pubs.acs.org/doi/10.1021/acsami.2c00532.

Additional photographs (Figures S1 and S4); singlet oxygen generation test (Figure S2); measurement of the loss methylene blue (Table S1 and Figure S3); and additional hematoxylin and eosin staining microscopic images (Figure S5) (PDF)

■ AUTHOR INFORMATION

Corresponding Authors

Kun Na − *Department of Biotechnology, Department of Biomedical-Chemical Engineering, The Catholic University of Korea, Gyeonggi-do 14662, Republic of Korea;* orcid.org/0000-0002-9629-0289; Email: kna6997@catholic.ac.kr

Hwoon-Yong Jung − *Department of Gastroenterology, Asan Medical Center, University of Ulsan College of Medicine, Seoul 05505, Republic of Korea*; Email: hyjung@amc.seoul.kr

Jung-Hoon Park − *Biomedical Engineering Research Center, Asan Institute for Life Sciences, Asan Medical Center, Seoul 05505, Republic of Korea*; Email: jhparkz@amc.seoul.kr

Authors

Sanghee Lee − *Department of Biotechnology, Department of Biomedical-Chemical Engineering, The Catholic University of Korea, Gyeonggi-do 14662, Republic of Korea*

Ji Won Kim − *Biomedical Engineering Research Center, Asan Institute for Life Sciences, Asan Medical Center, Seoul 05505, Republic of Korea*

Jinhwan Park − *Department of Biotechnology, Department of Biomedical-Chemical Engineering, The Catholic University of Korea, Gyeonggi-do 14662, Republic of Korea*

Hee Kyong Na − *Department of Gastroenterology, Asan Medical Center, University of Ulsan College of Medicine, Seoul 05505, Republic of Korea*

Do Hoon Kim − *Department of Gastroenterology, Asan Medical Center, University of Ulsan College of Medicine, Seoul 05505, Republic of Korea*

Jin Hee Noh − *Department of Gastroenterology, Asan Medical Center, University of Ulsan College of Medicine, Seoul 05505, Republic of Korea*

Dae Sung Ryu − *Biomedical Engineering Research Center, Asan Institute for Life Sciences, Asan Medical Center, Seoul 05505, Republic of Korea*

Jae Myung Park − *Division of Gastroenterology, Department of Internal Medicine, Seoul St. Mary's Hospital, The Catholic University of Korea, Seoul 06591, South Korea*

Complete contact information is available at: https://pubs.acs.org/10.1021/acsami.2c00532

Author Contributions

⊥S.H.L., J.W.K., and J.H.P. contributed equally to this work.

Notes

The authors declare no competing financial interest.

■ ACKNOWLEDGMENTS

This work was supported by the Korea Medical Device Development Fund grant funded by the Korean government (the Ministry of Science and ICT, the Ministry of Trade, Industry and Energy, the Ministry of Health & Welfare, the Ministry of Food and Drug Safety) (Project Number: 1711137983, KMDF_PR_20200901_0036) and research funds from the Catholic University of Korea (Research Fund 2021).

■ ABBREVIATIONS

ISD, intragastric satiety-inducing device
PDT, photodynamic therapy
MB, methylene blue
PS, photosensitizer

https://doi.org/10.1021/acsami.2c00532
ACS Appl. Mater. Interfaces XXXX, XXX, XXX−XXX

ROS, reactive oxygen species
TUNEL, transferase-mediated dUTP nick and labeling
TBWG, total body weight gain

REFERENCES

(1) Lee, P. C.; Dixon, J. Medical Devices for the Treatment of Obesity. *Nature Reviews Gastroenterology & Hepatology* **2017**, *14* (9), 553−564.
(2) Gadde, K.; Martin, C.; Berthoud, H.; Heymsfield, S. Pathophysiology and Management of Obesity. *J. Am. Coll Cardiol* **2018**, *71* (1), 69−84.
(3) Carrano, F. M.; Peev, M. P.; Saunders, J. K.; Melis, M.; Tognoni, V.; Di Lorenzo, N. The Role of Minimally Invasive and Endoscopic Technologies in Morbid Obesity Treatment: Review and Critical Appraisal of the Current Clinical Practice. *Obesity surgery* **2020**, *30* (2), 736−752.
(4) Tsesmeli, N.; Coumaros, D. Review of Endoscopic Devices for Weight Reduction: Old and New Balloons and Implantable Prostheses. *Endoscopy* **2009**, *41* (12), 1082−1089.
(5) Choi, Y. I.; Kim, K. O. Experimental Gastric Non-balloon Devices. *Clinical endoscopy* **2018**, *51* (5), 420.
(6) Kushner, R. F. Weight Loss Strategies for Treatment of Obesity. *Progress in cardiovascular diseases* **2014**, *56* (4), 465−472.
(7) Dayyeh, B. K. A.; Kumar, N.; Edmundowicz, S. A.; Jonnalagadda, S.; Larsen, M.; Sullivan, S.; Thompson, C. C.; Banerjee, S. ASGE Bariatric Endoscopy Task Force Systematic Review and Meta-analysis Assessing the ASGE PIVI Thresholds for Adopting Endoscopic Bariatric Therapies. *Gastrointestinal endoscopy* **2015**, *82* (3), 425−438. e5.
(8) Betzel, B.; Drenth, J. P.; Siersema, P. D. Adverse Events of the Duodenal-jejunal Bypass Liner: a Systematic Review. *Obesity surgery* **2018**, *28* (11), 3669−3677.
(9) Park, J.-H.; Bakheet, N.; Na, H. K.; Jeon, J. Y.; Yoon, S. H.; Kim, K. Y.; Zhe, W.; Kim, D. H.; Jung, H.-Y.; Song, H.-Y. A Novel Full Sense Device to Treat Obesity in a Porcine Model: Preliminary Results. *Obesity surgery* **2019**, *29* (5), 1521−1527.
(10) Bakheet, N.; Na, H. K.; Park, J.-H.; sung Ryu, D.; Jeon, J. Y.; Khashab, M. A.; Kumbhari, V.; Tsauo, J.; Song, H.-Y.; Hu, H. T. A Novel Intragastric Satiety-Inducing Device to Inhibit Weight Gain in Juvenile Pigs: a Pilot Study. *Obesity Surgery* **2020**, *30* (11), 4643−4651.
(11) Luo, Y.; Zhang, X.; Tsauo, J.; Jung, H.-Y.; Song, H.-Y.; Zhao, H.; Li, J.; Gong, T.; Song, P.; Li, X. Intragastric Satiety-Inducing Device Reduces Food Intake and Suppresses Body Weight Gain in a Rodent Model. *Surgical endoscopy* **2021**, *35* (3), 1052−1057.
(12) Kojima, M.; Hosoda, H.; Date, Y.; Nakazato, M.; Matsuo, H.; Kangawa, K. Ghrelin is a Growth-Hormone-Releasing Acylated Peptide from Stomach. *Nature* **1999**, *402* (6762), 656−660.
(13) Müller, T. D.; Nogueiras, R.; Andermann, M. L.; Andrews, Z. B.; Anker, S. D.; Argente, J.; Batterham, R. L.; Benoit, S.; Bowers, C. Y.; Broglio, F. Ghrelin. *Mol. Metab.* **2015**, *4* (6), 437−460.
(14) Tschop, M.; Smiley, D. L.; Heiman, M. L. Ghrelin Induces Adiposity in Rodents. *Nature* **2000**, *407*, 908−913.
(15) Maksud, F.; Alves, J. S.; Diniz, M.; Barbosa, A. Density of Ghrelin-Producing Cells is Higher in the Gastric Mucosa of Morbidly Obese Patients. *European journal of endocrinology* **2011**, *165* (1), 57−62.
(16) Tanaka-Shintani, M.; Watanabe, M. Distribution of Ghrelin-Immunoreactive Cells in Human Gastric Mucosa: Comparison With That of Parietal Cells. *Journal of gastroenterology* **2005**, *40* (4), 345−349.
(17) Wren, A.; Small, C.; Ward, H.; Murphy, K.; Dakin, C.; Taheri, S.; Kennedy, A.; Roberts, G.; Morgan, D.; Ghatei, M. The Novel Hypothalamic Peptide Ghrelin Stimulates Food Intake and Growth Hormone Secretion. *Endocrinology* **2000**, *141* (11), 4325−4328.
(18) Brown, S. B.; Brown, E. A.; Walker, I. The Present and Future Role of Photodynamic Therapy in Cancer Treatment. *lancet oncology* **2004**, *5* (8), 497−508.
(19) Moan, J. On the Diffusion Length of Singlet Oxygen in Cells and Tissues. *Journal of Photochemistry and Photobiology B: Biology* **1990**, *6* (3), 343−344.
(20) Castano, A. P.; Demidova, T. N.; Hamblin, M. R. Mechanisms in Photodynamic Therapy: Part Two Cellular Signaling, Cell Metabolism and Modes of Cell Death. *Photodiagnosis and photodynamic therapy* **2005**, *2* (1), 1−23.
(21) Luksiene, Z. Photodynamic Therapy: Mechanism of Action and Ways to Improve the Efficiency of Treatment. *Medicina (Kaunas, Lithuania)* **2003**, *39* (12), 1137−1150. PMID: 14704501
(22) Kessel, D.; Oleinick, N. L., Photodynamic Therapy and Cell Death Pathways. In *Photodynamic Therapy*; Springer, 2010; pp 35−46. DOI: 10.1007/978-1-60761-697-9_3.
(23) Wright, R. O.; Lewander, W. J.; Woolf, A. D. Methemoglobinemia: Etiology, Pharmacology, and Clinical Management. *Annals of emergency medicine* **1999**, *34* (5), 646−656.
(24) Ashkenazi, S. Photoacoustic Lifetime Imaging of Dissolved Oxygen Using Methylene Blue. *Journal of biomedical optics* **2010**, *15* (4), 040501.
(25) Orth, K.; Beck, G.; Genze, F.; Rück, A. Methylene Blue Mediated Photodynamic Therapy in Experimental Colorectal Tumors in Mice. *Journal of Photochemistry and Photobiology B: Biology* **2000**, *57* (2−3), 186−192.
(26) Wagner, M.; Suarez, E.; Theodoro, T.; Machado Filho, C.; Gama, M.; Tardivo, J.; Paschoal, F.; Pinhal, M. Methylene Blue Photodynamic Therapy in Malignant Melanoma Decreases Expression of Proliferating Cell Nuclear Antigen and Heparanases. *Clinical and Experimental Dermatology: Experimental dermatology* **2012**, *37* (5), 527−533.
(27) Tardivo, J. P.; Del Giglio, A.; De Oliveira, C. S.; Gabrielli, D. S.; Junqueira, H. C.; Tada, D. B.; Severino, D.; de Fátima Turchiello, R.; Baptista, M. S. Methylene Blue in Photodynamic Therapy: From Basic Mechanisms to Clinical Applications. *Photodiagn. Photodyn. Ther.* **2005**, *2* (3), 175−191.
(28) Olliver, J.; Wild, C.; Sahay, P.; Dexter, S.; Hardie, L. Chromoendoscopy with Methylene Blue and Associated DNA Damage in Barrett's Oesophagus. *Lancet* **2003**, *362* (9381), 373−374.
(29) Rzany, A.; Schaldach, M. Smart Material Silicon Carbide: Reduced Activation of Cells and Proteins on a-SiC: H-Coated Stainless Steel. *Prog. Biomed. Res.* **2001**, *6*, 182−194.
(30) Unverdorben, M.; Sippel, B.; Degenhardt, R.; Sattler, K.; Fries, R.; Abt, B.; Wagner, E.; Koehler, H.; Daemgen, G.; Scholz, M. Comparison of a Silicon Carbide-Coated Stent Versus a Noncoated Stent in Human Beings: the Tenax Versus Nir Stent Study's Long-term Outcome. *Am. Heart J.* **2003**, *145* (4), E17.
(31) Melgoza, D.; Hernández-Ramírez, A.; Peralta-Hernández, J. Comparative Efficiencies of the Decolourisation of Methylene Blue Using Fenton's and Photo-Fenton's Reactions. *Photochemical & Photobiological Sciences* **2009**, *8* (5), 596−599.
(32) Kofler, B.; Romani, A.; Pritz, C.; Steinbichler, T. B.; Schartinger, V. H.; Riechelmann, H.; Dudas, J. Photodynamic Effect of Methylene Blue and Low Level Laser Radiation in Head and Neck Squamous Cell Carcinoma Cell Lines. *International journal of molecular sciences* **2018**, *19* (4), 1107.
(33) Baier, J.; Maier, M.; Engl, R.; Landthaler, M.; Bäumler, W. Time-Resolved Investigations of Singlet Oxygen Luminescence in Water, in Phosphatidylcholine, and in Aqueous Suspensions of Phosphatidylcholine or HT29 Cells. *J. Phys. Chem. B* **2005**, *109* (7), 3041−3046.
(34) Zebger, I.; Snyder, J. W.; Andersen, L. K.; Poulsen, L.; Gao, Z.; Lambert, J. D.; Kristiansen, U.; Ogilby, P. R. Rapid Communication: Direct Optical Detection of Singlet Oxygen from a Single Cell. *Photochemistry and photobiology* **2004**, *79* (4), 319−322.
(35) Wilkinson, F.; Helman, W. P.; Ross, A. B. Rate Constants for the Decay and Reactions of the Lowest Electronically Excited Singlet State of Molecular Oxygen in Solution. An Expanded and Revised Compilation. *J. Phys. Chem. Ref. Data* **1995**, *24* (2), 663−677.
(36) Bae, B.-c.; Yang, S.-G.; Jeong, S.; Lee, D. H.; Na, K.; Kim, J. M.; Costamagna, G.; Kozarek, R. A.; Isayama, H.; Deviere, J. Polymeric

https://doi.org/10.1021/acsami.2c00532
ACS Appl. Mater. Interfaces XXXX, XXX, XXX−XXX

Photosensitizer-Embedded Self-Expanding Metal Stent for Repeatable Endoscopic Photodynamic Therapy of Cholangiocarcinoma. *Biomaterials* **2014**, *35* (30), 8487−8495.
(37) Han, J.; Hwang, H. S.; Na, K. TRAIL-Secreting Human Mesenchymal Stem Cells Engineered by a Non-Viral Vector and Photochemical Internalization for Pancreatic Cancer Gene Therapy. *Biomaterials* **2018**, *182*, 259−268.
(38) Hayashida, T.; Murakami, K.; Mogi, K.; Nishihara, M.; Nakazato, M.; Mondal, M. S.; Horii, Y.; Kojima, M.; Kangawa, K.; Murakami, N. Ghrelin in Domestic Animals: Distribution in Stomach and its Possible Role. *Domestic Animal Endocrinology* **2001**, *21* (1), 17−24.
(39) Takiguchi, S.; Adachi, S.; Yamamoto, K.; Morii, E.; Miyata, H.; Nakajima, K.; Yamasaki, M.; Kangawa, K.; Mori, M.; Doki, Y. Mapping Analysis of Ghrelin Producing Cells in the Human Stomach Associated With Chronic Gastritis and Early Cancers. *Digestive diseases and sciences* **2012**, *57* (5), 1238−1246.
(40) Arepally, A.; Barnett, B. P.; Montgomery, E.; Patel, T. H. Catheter-Directed Gastric Artery Chemical Embolization for Modulation of Systemic Ghrelin Levels in a Porcine Model: Initial Experience. *Radiology* **2007**, *244* (1), 138−143.
(41) Paxton, B. E.; Kim, C. Y.; Alley, C. L.; Crow, J. H.; Balmadrid, B.; Keith, C. G.; Kankotia, R. J.; Stinnett, S.; Arepally, A. Bariatric Embolization for Suppression of the Hunger Hormone Ghrelin in a Porcine Model. *Radiology* **2013**, *266* (2), 471−479.

https://doi.org/10.1021/acsami.2c00532
ACS Appl. Mater. Interfaces XXXX, XXX, XXX−XXX